Numerical simulation of a large scale magnetized inductively coupled plasma generator using COMSOL

Donglin Liu (刘东林)[1], Xiaoping Li (李小平)[1], Fan Lei (雷凡) [a)1], Yanming Liu (刘彦明)[1], JiahaoXu (徐佳皓)[1] and Xi Chen (陈曦)[1]

[1]*School of Aerospace Science and Technology, Xidian University, Xi'an Shaanxi 710071, China*

Abstract

It has already been demonstrated that fluid models can be used to simulate two-dimensional axisymmetric inductively coupled plasma via implementation in the COMSOL (multi-physics simulation software) platform. In this study, we improved the model and simulated a large scale magnetized inductively coupled plasma generator filled with argon to study the effect of the static magnetized field on inductively coupled plasma discharges. In fact, before the static magnetized field is applied, the electron transport mobility is isotropic; and after the static magnetized field is applied, the electron transport mobility is anisotropic. Distributions of the number density and temperature of electrons were obtained for various input powers, pressures, and magnetized field configurations. In addition, the macro-gas temperature distribution was obtained for different magnetized field configurations. There are four multiphysics coupling interfaces in our simulation model, namely the ICP discharge interface, static magnetized field interface, laminar Flow interface, and heat transfer in fluids interface, they achieve the mutual coupling via the related physical quantities. We conclude that the distributions of the number density of the electrons can be improved by the addition of a static magnetized field.

Keywords: ICP discharge, Magnetized inductively coupled plasma discharge, COMSOL simulation

1. Introduction

In view of the aircraft flying in the near space, the aircraft will produce a "plasma sheath" on its surface, and then "communications blackout" is generated. In order to simulate the real plasma environment and represent the real environment of near space on the ground, the high density plasma

[a)]leifan_study@126.com

generation methods have been put forward over years. ICP(inductively coupled plasma) discharge is widely used for its no pollution and non-contact features, in order to further improve the electron density, the method of static magnetized field is thought by people, the helicon is a successful application. Helicon discharge is a concept put forward in 1960, it is used for experiment for low frequency electromagnetic waves propagating in high conductivity media, such as low-temperature metals in a magnetized field or gas discharge plasma[1-2] with the power supply frequency of 13.56 MHz. In the 1970s, new radiofrequency magnetized plasma sources were put forward by Boswell at the Australian National University. Boswell present a simple description of helicon propagation characteristics in free and bounded plasmas with the power supply frequency 13.56 MHz.[3-4] In fact, helicon discharges have been applied in aerospace industries, for industrial applications, and for basic plasma research (F. F. Chen and Shoji).[4-5] Helicon discharge technologies have several advantages, namely high ionization efficiencies, high electron densities, low magnetized fields, and simple structures. The helicon discharge is a very efficient plasma source, the radiofrequency waves produced by the antenna are coupled to the spiral waves propagating through the plasma, and then providing energy to the plasma, finally, the high density is generated. However, MICP(magnetized inductively coupled plasma) discharges considered in this study have a significant difference from helicon discharge in physical mechanism of discharge. The MICP's power supply frequency is 440 kHz, and the size of our MICP(large scale size) is different from them, the helicon can't form in such size and frequency, so the mode of wave propagation is also different.

In recent years, there has been the little research in simulations of discharges applying stastic magnetized field. T. Lafleur, C. Charles et al. used the comprehensive model to study the physical characteristics of helicon plasma.[3] Meanwhile, R. W. Boswell et al. used the PIC-MCC model to study the physical characteristics of helicon plasma. Further L. Chang, and M. J. Hole et al. used the two-fluid model to study the electric field and magnetized field characteristic of helicon plasma.[6] However, the industrial frequency of 13.56 MHz was applied in their models; but we use a frequency of 440 kHz because the maximum output power of the medium-frequency power supply of our equipment was 1 MW and its frequency was 440 kHz; importantly for us, the power supply's electromagnetic shielding was easy to handle. In addition, there is a big difference between their models and our model in both the shape and size of the model. The helicon simulation and ICP simulation methods are combined in my

paper, and a new simulation theory is put forward, then the static magnetized field is applied on the basis of ICP simulation, the diffusion coefficient is set the anisotropic, the simulation methods are based on this theory in our MICP simulation. Finally, the results from the simulations in this paper were compared with the results of an inductively coupled plasma generator simulation by F. Lei et al. reported in the literature[7], the electron density increased with almost an order of magnitude. We conducted simulations for relatively simple discharge chemistries in this paper, namely, for argon (Ar).

In this paper, Section 2 presents the theoretical basis of the fluid plasma model of MICP, and the numerical simulation is described in detail. In Section 3, the argon MICP discharge in the simulation based on COMSOL is presented. Finally, Section 4 presents our concluding remarks.

2. Plasma Model Formulation

Different equations are provided to describe the behavior of the electrons, ions, and neutrals in an argon plasma discharge, each of which obey six important conservations and relative theories, electromagnetic field equations for the static magnetized field, mass conservation equations, electron energy equations, electromagnetic field equations, Navier–Stokes equations for the neutral background gas, and heat transfer equation for the heavy gas temperature, the several major parts are described next, a small number of theories are the same as ICP simulation in F. Lei[7], but there are some differences.

2.1. Electromagnetic field equations for the static magnetized field

And in our MICP model, a static magnetized field is applied to the inductively coupled plasma (ICP) discharge, and the electromagnetic field equations for the static magnetized field are

$$\nabla \times H = J, \tag{1}$$

$$\nabla \times A = B, \tag{2}$$

$$B = \mu_0 H, \tag{3}$$

where H is the magnetized field intensity, B is the magnetized flux density, A is the vector potential, σ is the plasma electrical conductivity, μ_0 is the magnetized permeability of free space.

In our model, the electron transport mobility and diffusion coefficient is an important parameter, before the static magnetic field is applied, the electron transport mobility and diffusion coefficient is

isotropic; after the static magnetic field is applied, the electron transport mobility and diffusion coefficient become anisotropic.

The diffusion coefficient along the magnetic field line is same as those in the isotropic case. The diffusion coefficient perpendicular to the magnetic field line is function of cyclone frequency, as shown below.

$$D_{\parallel} = \frac{kT_e}{m_e \nu}, \tag{4}$$

$$D_{\perp} = \frac{D_{\parallel}}{1+(\omega_c/\nu)^2}, \tag{5}$$

$$\omega_c = \frac{q \times B}{m_e}, \tag{6}$$

where ν is the collision frequency, B is the magnetic flux density, q is the quantity of electron charge, m_e is electron mass.

Generally, the magnetic field line depends on the coil shape and is not always in the r or z direction, so it is necessary to convert the coordinate system along the magnetic field line to the cylindrical coordinate system, as shown in the Figure 1. The coordinate r and z can be replaced with x' and y' in the following Eq. (7), φ is the angle between the z and x'.

$$r = x'\sin\varphi + y'\cos\varphi \qquad z = x'\cos\varphi - y'\sin\varphi, \tag{7}$$

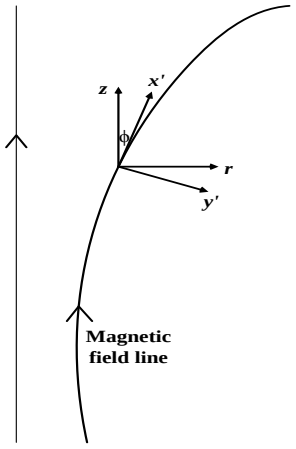

Figure 1. Converting of coordinate system along magnetic field line to cylindrical coordinate system

The anisotropic diffusion coefficient is then derived as below.

$$D_e = \begin{pmatrix} D_{\parallel} \bullet \sin^2\varphi + D_{\perp} \bullet \cos^2\varphi & \sin\varphi \bullet \cos\varphi \bullet (D_{\parallel} - D_{\perp}) \\ \sin\varphi \bullet \cos\varphi \bullet (D_{\parallel} - D_{\perp}) & D_{\parallel} \bullet \cos^2\varphi + D_{\perp} \bullet \sin^2\varphi \end{pmatrix} \tag{8}$$

2.2. Mass conservation equations

The electron density is computed by solving the drift-diffusion equation for the electron density.

$$\frac{\partial n_e}{\partial t} + \nabla \bullet \Gamma_e = R_e - (u \bullet \nabla) n_e, \tag{9}$$

where n_e is the electron number density and Γ_e is the electron flux, u is the neutral fluid velocity. And R_e is determined by the product of the reaction electron number density and the coefficient of the reaction rate,

$$\mathrm{R}_e = \sum_{j=1}^{M} x_j k_j(T_e) N_n n_e, \tag{10}$$

where x_j is the mole fraction of the target species for reaction j, $k_j(T_e)$ is the rate coefficient for reaction j (m^3/s), which is a function of the electron temperature, it is calculated in Ref.[8, 9]. The important collision parameter values for argon plasma were obtained from Ref. [10, 11]. N_n is the total neutral number density ($1/m^3$).

The drift-diffusion approximation is used to describe the electron fluxes; it is given by

$$\Gamma_e = -(\mu_e \bullet E) n_e - D_e \bullet \nabla n_e, \tag{11}$$

where μ_e is the drift mobility of electron and where D_e is the diffusion coefficient of the electron given by equation (8). In addition, the electric field E here is the high frequency electric field, it includes the electric field on the driving coil and the electric field generated by the plasma. It is given by Eq.(12).

$$E = -\frac{\partial A}{\partial t}, \tag{12}$$

where the A is the vector potential obtained from section 2.4.

For non-electron species, the following equation is solved for the mass fraction of each species.

$$\rho \frac{\partial}{\partial t}(w_k) + \rho(u \bullet \nabla) w_k = \nabla \bullet j_k + R_k, \tag{13}$$

where the $\rho(kg/m^3)$ is the quality of the mixture density, $R_k(kg/(m^3*s))$ is the chemical reactions of particles, w_k is the mass fraction of the solving particle, and $u(m/s)$ is the velocity, j_k is the diffusion flux vector.

2.3. Electron energy equations

In our model, the electron energy is given by

$$\frac{\partial n_\varepsilon}{\partial t} + \nabla \bullet \Gamma_\varepsilon + E \bullet \Gamma_e = R_\varepsilon - (u \bullet \nabla) n_\varepsilon , \tag{15}$$

$$\Gamma_\varepsilon = -(\mu_\varepsilon \bullet E) n_\varepsilon - D_\varepsilon \bullet \nabla n_\varepsilon , \tag{16}$$

where E is the high frequency electric field, where n_ε is the electron energy density, μ_ε is the electron energy mobility and Γ_ε is the electron energy flux, R_ε is determined by the product of the reaction electron number density and the coefficient of the reaction rate, and the energy loss from reaction.

$$\mathrm{R}_\varepsilon = \sum_{j=1}^{P} x_j k_j(T_e) N_n n_e \Delta\varepsilon_j , \tag{17}$$

where $\triangle\varepsilon_j$ the energy loss from reaction(V). The electron mobility, electron energy diffusion coefficient and electron energy mobility are then calculated using

$$\mu_e = \frac{D_e}{T_e} , \tag{18}$$

$$\mu_\varepsilon = (\frac{5}{3})\mu_e , \tag{19}$$

$$D_\varepsilon = \mu_\varepsilon T_e , \tag{20}$$

2.4. Electromagnetic field equations for high frequency field

In the two-dimensional axisymmetric MICP model, the Maxwell electromagnetic field equation is

$$\nabla^2 A - i\omega\mu_0\sigma A + \mu_0 j_{coil} = 0 , \tag{21}$$

$$\sigma = \frac{q^2 n_e}{m_e(\nu_e + j\omega)} , \tag{22}$$

where j_{coil} is the electric current density in the driving coil σ is the plasma electrical conductivity, ν_e is the electron collision frequency and ω ($\omega = 2\pi f$) is the angular frequency, where f is the frequency of the electromagnetic field.

2.5. Navier–Stokes equations and Heat transfer equations for the neutral background gas

The neutral background gas has an important influence on the plasma distribution. First, the reaction rate is proportional to the number density of the neutral gas. Second, the energy and mass convection of

particles is also influenced by the flow velocity. The neutral background gas density and flow velocity can be obtained by solving the Navier–Stokes equations and heat transfer equations (for the temperature) which are same as those in Ref.[7]. To avoid repetition, it's not described in this article.

Equations (1)-(22) are together solved using a finite element method as formulated in the COMSOL software package.[12-19]

3. Results and discussions

3.1. COMSOL model of the argon MICP generator

Based on the simulation results of F. Lei, X. Li et al. on ICP generator,[7] the new results with the static magnetized field added can be obtained. The COMSOL model of the argon MICP generator is a two-dimensional axisymmetric structure with the ICP generator adding a static magnetized field. The dimensions are given in detail in Figure 2. There are four copper turns in our model and eight copper turns in the ICP model, and the diameter of the copper coils section was 0.01m. A circular spiral coil was supplied with a 440kHz radio frequency input power above a quartz pipe to generate plasma at different pressures. In this study, three sets of conditions were used in the simulations: 1) a fixed pressure of 5 Pa and a variable input power (600 to 1000 W); 2) a fixed power input of 800W and variable pressure (2 to 10 Pa); and 3) a fixed power input of 1000W, a fixed pressure of 5 Pa, and a static magnetized field varying from ~0.01 to ~0.1 T. In addition, the initial boundary conditions were set as follows:

1) initial electron density of 10^{15} m^{-3};

2) an average electron energy of 3V, and a temperature of 300K;

3) electron mobility was set to anisotropic, and was given as different parameters;

4) argon flow rate at the inlet channel was fixed at 0.66g/s (the air inflow was stable in the end).

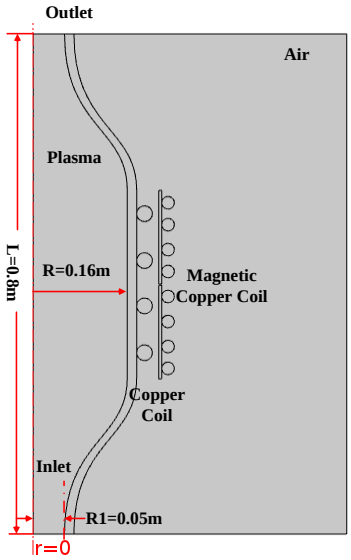

Figure 2. Two-dimensional axisymmetric structure of the MICP generator.

Regarding the astringency and the calculated accuracy of the MICP model, the all computational domain was divided into an irregular grid of 23265 triangles. The minimum element quality of the mesh was $5.843e^{-3}$, while the average element quality of the mesh was 0.8829. The two-dimensional geometry and irregular grid of the MICP generator is shown in Figure 3.

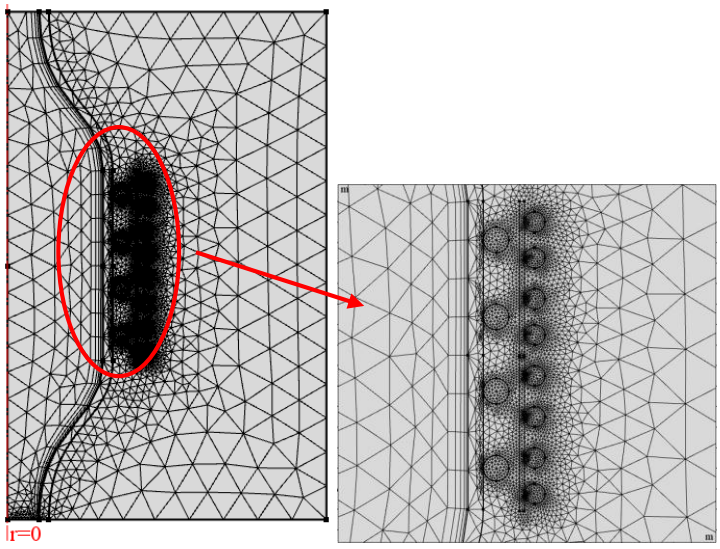

Figure 3. Geometry and grid of the MICP generator.

The boundary conditions on the walls are very important for the plasma distribution in the MICP model simulation, as given,

1) the boundary condition on the walls is no voltage (*V=0*);

2) the boundary condition of thermal emission flux(Γ_t) on the walls is set to zero, the boundary condition of ion flux(Γ_i) on the walls is set to zero, and the boundary condition of the mean thermionic energy of an electron(ε) on the walls is set to zero as follows in Ref.[7].

3) the boundary conditions on the walls for the excited-state particles produce a chemical reaction and form the neutral ground state particles and the secondary electron emission coefficient(γ_i) is zero; in addition, the mean energy of a secondary electron (ε_i) is zero on the walls;

4) the boundary conditions of the inlet and outlet are set to velocity inlet type and pressure outlet, respectively, and the wall boundary condition is simply defined with the Dirichlet condition, which is $u=0$;

5) the boundary conditions on the walls is no slip$(u=0)$ in the laminar flow model;

6) the temperature of the boundary conditions on the walls in the heat transfer model is set to 300K.

There are four multiphysics coupling interfaces in our simulation model, namely the ICP discharge interface, static magnetized field interface, Laminar Flow interface, and Heat transfer in Fluids interface. In general, the four multiphysics coupling interfaces can achieve coupling via the related physical quantities, and the specific coupling relationships are described in Ref.[7].

3.2. Simulation results

3.2.1. Influence of different static magnetized field for each parameter

From the different parameter distributions obtained from the MICP model for the static magnetized field of ~0.01T[Figure 4(a)], the maximum value of the electron density was found to be ~8.82 $\times 10^{18}$ m^{-3}[Figure 4(b)] in the core region; the maximum value of the electron temperature was ~3.16 eV[Figure 4(c)], and the maximum value of the macro-gas temperature was ~714 K[Figure 4(d)]. For a static magnetized field of ~0.05T[Figure 5(a)], the maximum value of the electron density was ~3.54 $\times$ $10^{19}m^{-3}$[Figure 5(b)] in the core region; the maximum value of the electron temperature was ~4.64 eV[Figure 5(c)], and the maximum value of macro-gas temperature was ~845 K[Figure 5(d)]. For the static magnetized field of ~0.1 T[Figure 6(a)],the maximum value of the electron density was ~4.01 $\times$ 10^{19} m^{-3}[Figure 6(b)] in the core region; the maximum value of the electron temperature was ~5 eV[Figure 6(c)], and the maximum value of the macro-gas temperature was ~852 K[Figure 6(d)]. The

various parameters (electron density, electron temperature, and macro-gas temperature) increase with increasing static magnetized field strength. The electrons keep speeding up with as the static magnetized field strength is increased, as the static magnetized field injects ever more energy to produce further electrons, and the various parameter(electron density, electron temperature, and macro-gas temperature) increase to high levels.

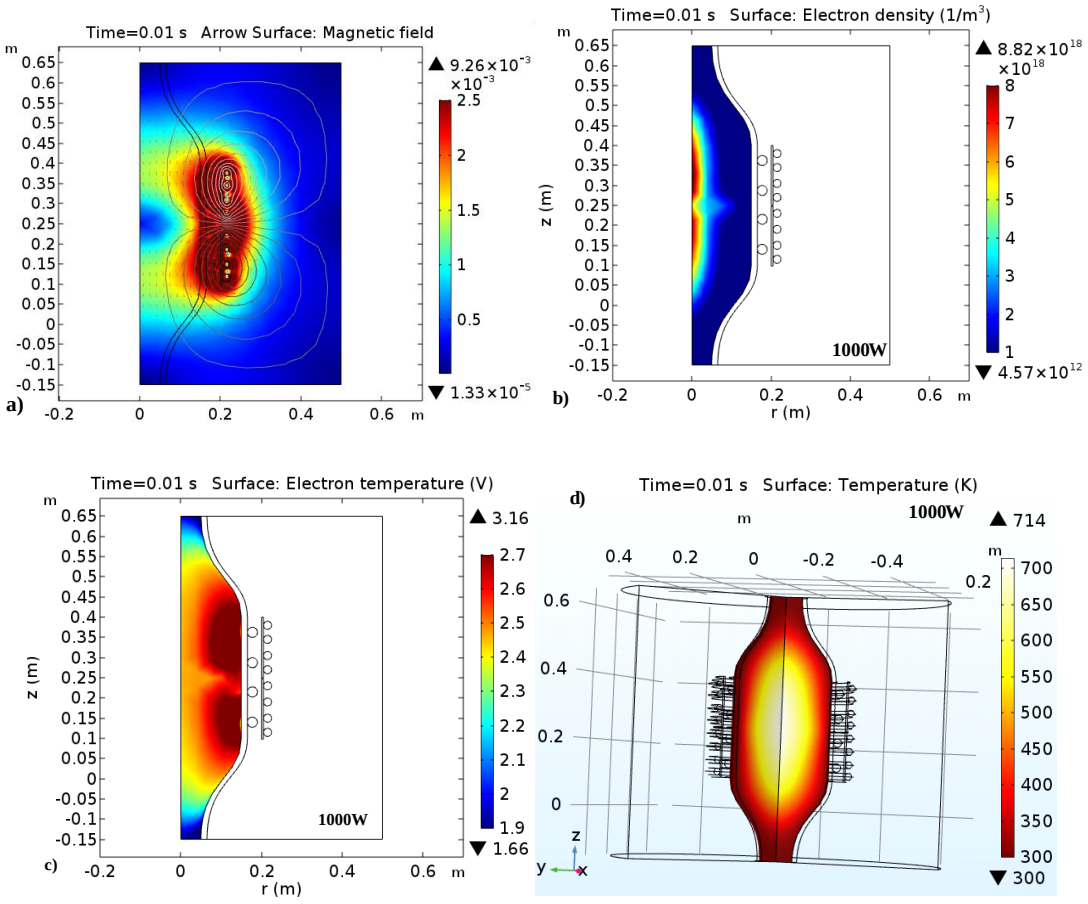

Figure 4. Distribution of the various parameters of the static magnetized field at ~0.01T at a fixed input power of 1000 W and a pressure of 5Pa: a) static magnetized field distribution, b) electron density distribution, c) electron temperature distribution, and d) macro-gas temperature distribution.

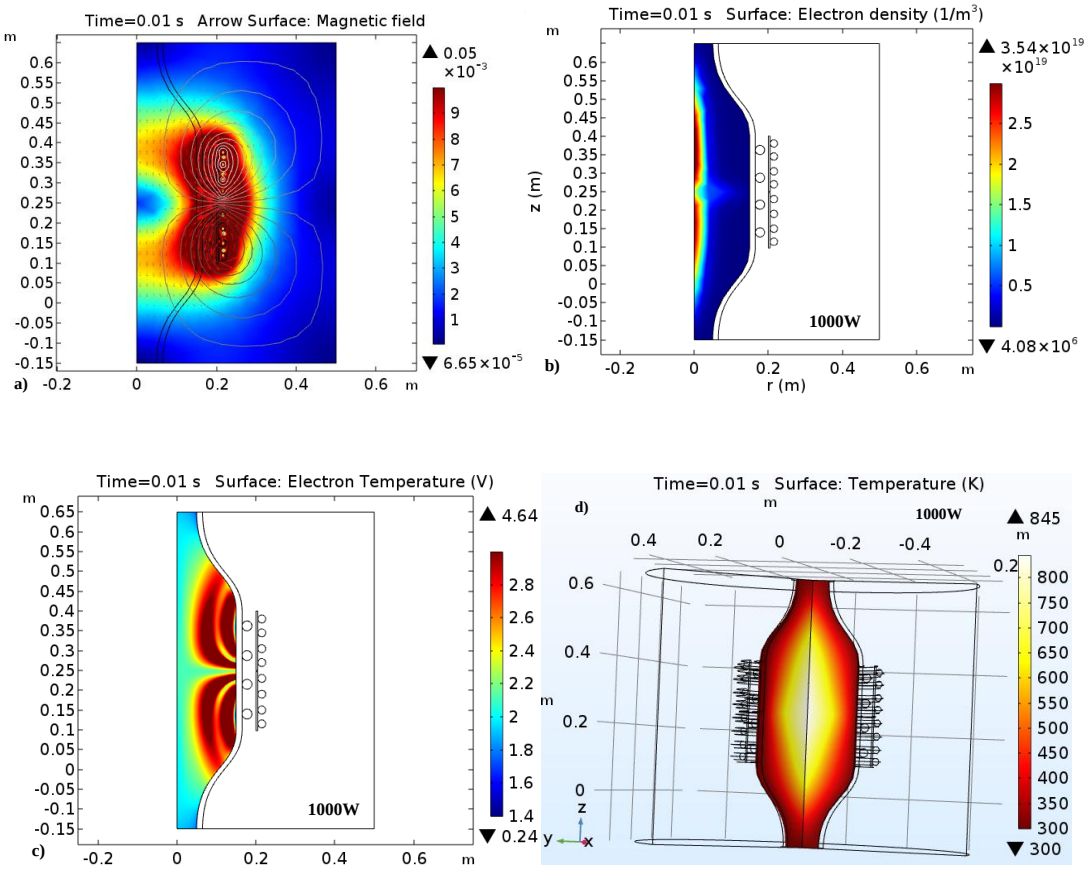

Figure 5. Distribution of the various parameters of the static magnetized field at ~0.05T at a fixed input power of 1000 W and a pressure of 5Pa: a) static magnetized field distribution, b) electron density distribution, c) electron temperature distribution, and d) macro-gas temperature distribution.

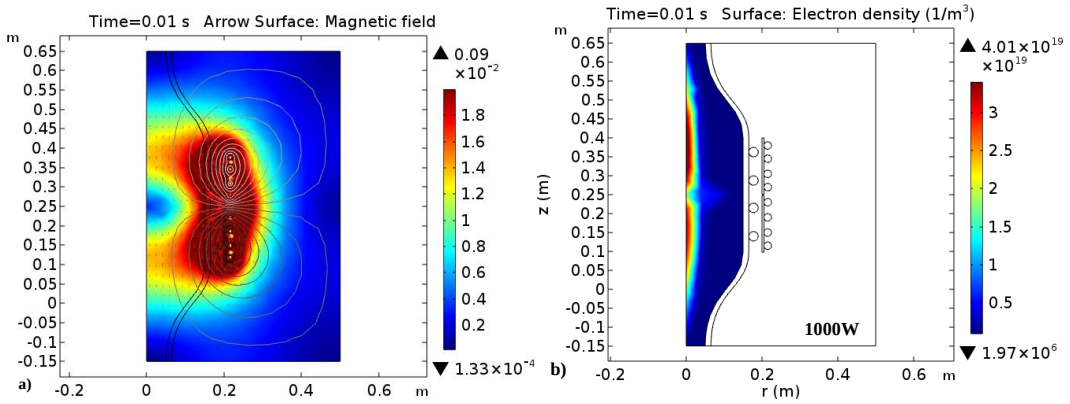

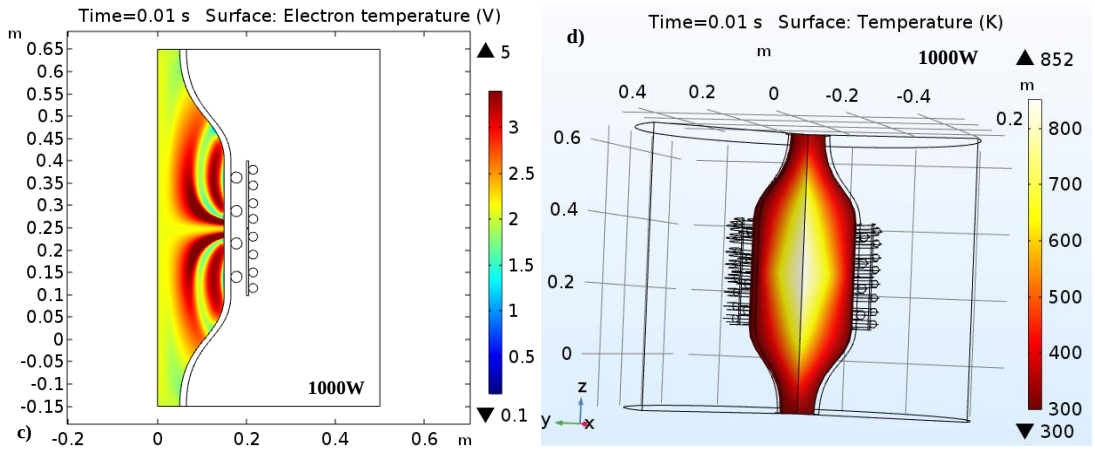

Figure 6. Distribution of the various parameters of the static magnetized field at ~0.1T at a fixed input power of 1000 W and a pressure of 5Pa: a) static magnetized field distribution, b) electron density distribution, c) electron temperature distribution, and d) macro-gas temperature distribution.

3.2.2. Different power inputs with the ~0.01T

Some results of the ICP model were obtained in our previous simulation, but now the electron density distributions obtained for the MICP model at a fixed pressure of 5 Pa, an added static magnetized field of ~0.01T [Figure 4(a)], and different power inputs [Figure 7(a)–(c)] show that the maximum values were attained in the core region, the increasing trend in the electron density is similar to the electron density of ICP. The comparison diagram of electron density changing trend between MICP and ICP with different power supplies is given as Figure 8, the electron density of ICP in Figure 8 is from Ref.[7], and the electron density increases along with the power(the electron density of MICP is bigger than the electron density of ICP). As the degree of ionization increases along with the power, the electron density therefore also increases.

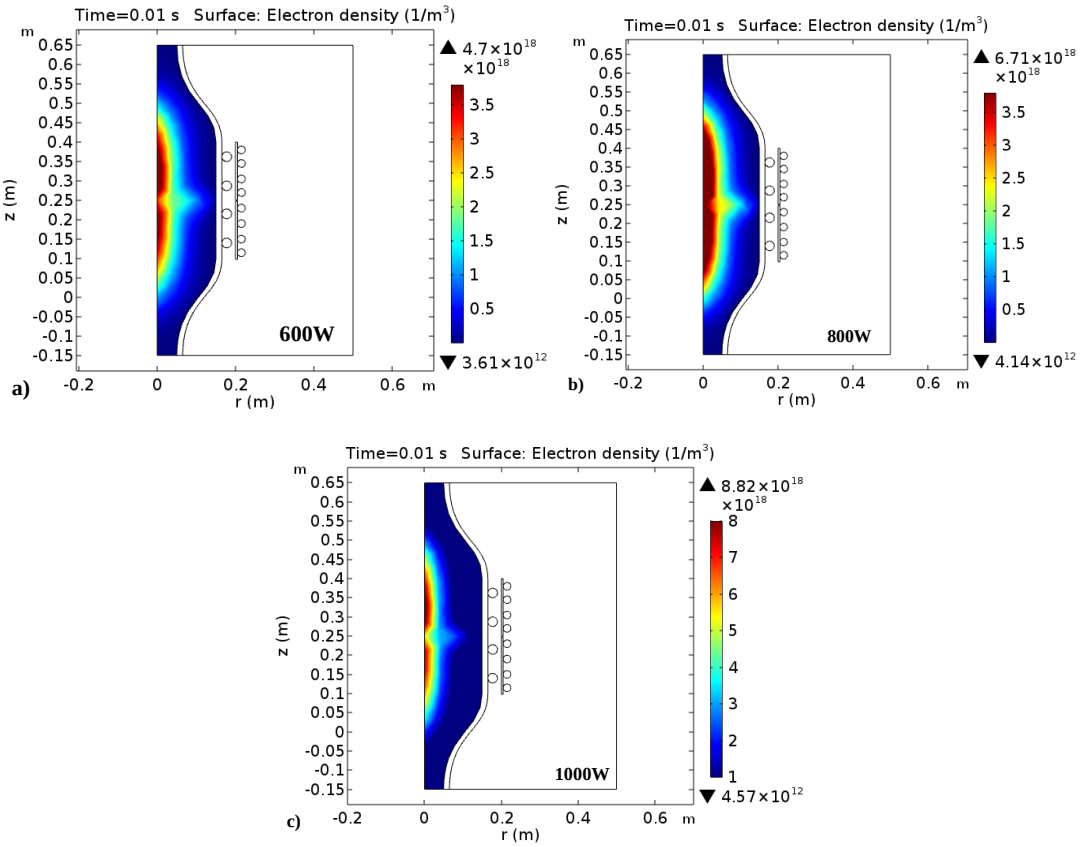

Figure 7. Power dependence of the electron density distribution at a fixed pressure of 5 Pa and with an added static magnetized field of ~0.01T: a) 600 W, b) 800 W, and c) 1000 W.

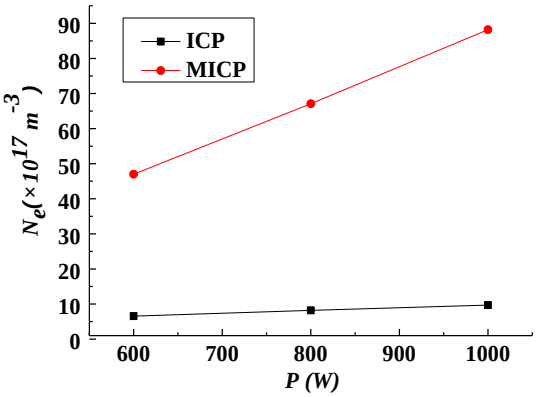

Figure 8. Comparison diagram of electron density changing trend between MICP and ICP with different power supplies

3.2.3. Different pressures with the ~0.01T

From the electron density distributions obtained from the MICP model for several fixed pressure values (Figure 9(a)–(c)),with the added static magnetized field of ~0.01T [Figure 4(a)] the maximum value attained for each setting were increasing in the core region. In addition, with increasing pressure, the electron density decreases for a fixed input power of 800W owing to less frequent particle collisions. The comparison diagram of electron density changing trend between MICP and ICP with different pressures is given as Figure 10, the electron density of ICP in Figure 10 is from Ref.[7]. The electron density of ICP increases along with the pressure, but the electron density of MICP decreases along with the pressure. The electron density of MICP is bigger than the electron density of ICP, and the electron density of therefore also increases.

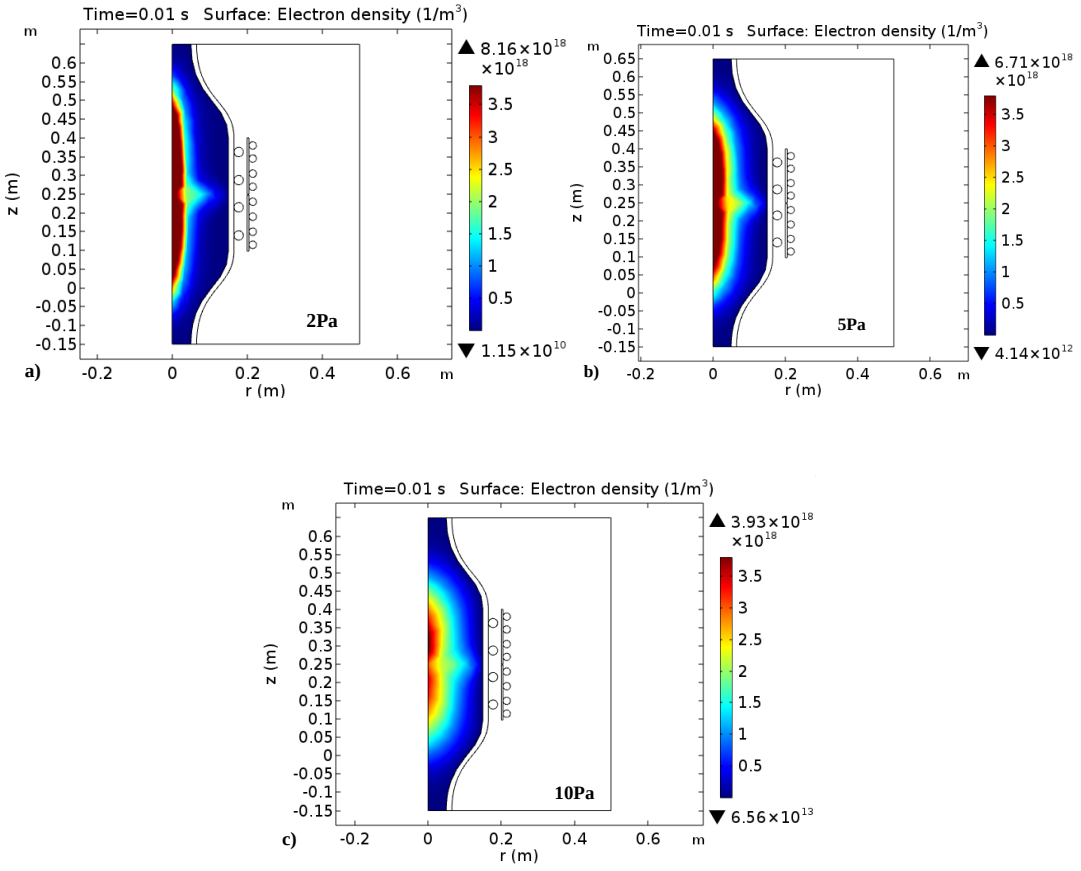

Figure 9. Pressure dependence of the electron density distribution at a fixed input power of 800 W and an added static magnetized field of ~0.01T: a) 2 Pa, b) 5 Pa, and c) 10 Pa.

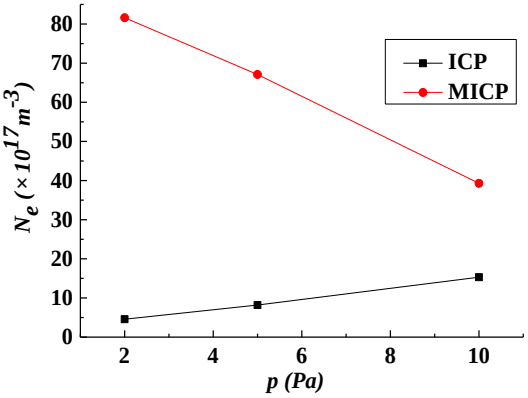

Figure 10. Comparison diagram of electron density changing trend between MICP and ICP with different pressures

4. Conclusions

The physical properties of a two-dimensional axisymmetric MICP model were studied using COMSOL software with different static magnetized field, different power, and pressure settings. To gain a better understanding of the dynamics in an argon MICP generator, the electron density, electron temperature, and macro-gas temperature were calculated inside an argon MICP generator with a frequency of 440kHz. The static magnetized field added in the ICP generator improves the electron density in this simulation, and the electron density increase with increasing static magnetized field strength. In addition, the electron density of MICP decreases along with the pressure, this phenomenon is contrary to the ICP. These results may help in future research towards developing a more effective method to improve the electron density of ICP generators. Finally, we can add the static magnetized field to conduct some related experiments and use those experimental results to verify the accuracy of our simulation in the future.

Acknowledgments

This work was supported in part by the Chinese National Natural Science Foundation, under Grant No. 61627901, and in part by the National Basic Research Program of China under Grant No. 2014CB340204 and in part by China Postdoctoral Science Foundation under Grant No. 2017M623119, and the National Defense Basic Scientific Research Program of China under Grant No.

JCKY2016110C040, the National Natural Science Foundation of China under Grant No. 61601353, the National Basic Research Program of China under Grant 2014CB340205, Shaanxi National Natural Science Foundation under Grant 2016JM06, the National Natural Science Foundation of China under Grant No.61701381, and in part by Aerospace T. T. &. C. Innovation Program, under Grant No. 201713B.

References

[1] A. F. Gibson, R. E. Burgess, P. Aigrain, C. Kittle, "Progress in Semiconductors," Physics Today, 1960, 11(6): 35-36.

[2]F. F. Chen, "The low-field density peak in helicon discharge," Physics of plasmas, 2013, 10(6): 2586-2592.

[3]T. Lafleur, C. Charies, R. W. Boswell, "Electron temperature characterization and power balance in a low magnetized field helicon mode," Journal of physics D Applied physics, 2011, 44(18): 185204.

[4]R. W. Boswell, F. F. Chen, "Helicon-The Early Years," IEEE Transactions on Plasma Science, 1997, 25(6): 1229-1244.

[5]G. N. Harding, P. C. Thonemann, "A study of helicon waves in indium," Proceedings of the Physical Society, 1965, 85(2): 317.

[6]L. Chang, M. J. Hole, and C. S. Corr. "A flowing plasma model to describe drift waves in a cylindrical helicon discharge," Physics of Plasmas, 2011, 18(4): 965.

[7]F. Lei, X. Li, Y. Liu, et al., "Simulation of a large size inductively coupled plasma generator and comparison with experimental data," AIP Advances, 2018, 8(1): 15003.

[8]Yamabe C., Buckman S.J.. "Measurement of free-free emission from low-energy-electron collisions with Ar," Physical Review A, 1983, 27: 1345-1352.

[9]Hagelaar GJM, Pitchford LC. "Solving the Boltzmann equation to obtain electron transport coefficients and rate coefficients for fluid models," Plasma Sources Sci. Technol., 2005, 14: 722-733.

[10]Lymberopoulos D. P., Economou D. J.. "Fluid simulations of glow discharges: Effect of metastable atoms in argon," J. Appl. Phys., 1993, 73(8): 3668.

[11]Angel Ochoa Brezmes, Cornelia Breitkopf. "Fast and reliable simulations of argon inductively coupled plasma using COMSOL," Vacuum, 2015, 16: 65-72.

[12]Cheng Jia, JiLinhong, Wang Kesheng, Han Chuankun, and Shi Yixiang. "Two-dimensional simulation of inductively coupled plasma based on COMSOL and comparison with experimental data," Journal of Semiconductors, 2013, 34(6): 066004.

[13]Lymberopoulos D. P., Economou D. J.. "Modeling of an inductively coupled plasma torch with argon at atmospheric pressure," Phys. Scr., 2014, 014008.

[14]Rauf S., Kushner M. J.. "Model for noncollisional heating in inductively coupled plasma processing sources," J. Phys D: Appl. Phys., 1997, 81(9): 5966.

[15]Economou D. J., Wise R. S., Kubota A. A.. "Plasmid formation and multiple steady states in a low pressure, inductively coupled electronegative plasma," IEEE T. Plasma Sci., 1999, 27(1): 60-61.

[16]Kushner M. J.. "Hybrid modeling of low temperature plasmas for fundamental investigations and equipment design," J. Phys. D: Appl. Phys., 2009, 42(19): 194013.

[17]Hammond E. P., Mahesh K. and Moin P.. "A numerical method to simulate radio frequency Plasma discharge," J. Comput. Phys., 2002, 176: 402-429.

[18]Cheng Jia, Ji Linhong, Zhu Yu, and Shi Yixiang. "Fluid model of inductively coupled plasma etcher based on COMSOL," Journal of Semiconductors, 2010, 31(3): 032004.

[19]J. F. Caneses, B. D. Blackwell, and P. Piotrowicz. "Helicon antenna radiation patterns in a high-density hydrogen linear plasma device," Physics of plasmas, 2017, 24: 113513-113537.